Chinese Chemical Letters 33 (2022) 4675–4678

Contents lists available at ScienceDirect

Chinese Chemical Letters

journal homepage: www.elsevier.com/locate/cclet

Synthesis, structure and properties of three novel transition-metal-containing tantalum-phosphate clusters

Xue Li, Hui Zhao, Yuyan Li, Yuanyuan Yang, Mingyang Zhang, Suyi Liu, Pengtao Ma, Jingping Wang*, Jingyang Niu*

Henan Key Laboratory of Polyxometalate Chemistry, College of Chemistry and Chemical Engineering, Henan University, Kaifeng 475004, China

ARTICLE INFO

Article history:
Received 2 December 2021
Revised 27 December 2021
Accepted 28 December 2021
Available online 4 January 2022

Keywords:
Polyoxotantalates
Transition-metal
Synthesize
Structure
Proton-conduction

ABSTRACT

Peroxide ligation of aqueous metal–oxo clusters provides rich speciation and structural diversity. Here, three novel transition-metal derivatives of polyoxometalate anions, $[Ni_2(H_2O)_{10}\{P_4Ta_6(O_2)_6O_{24}\}]^{6-}$ (**1a**), $[Zn(H_2O)_4\{P_4Ta_6(O_2)_6O_{24}\}]^{8-}$ (**2a**) and $[Cd(H_2O)_4\{P_4Ta_6(O_2)_6O_{24}\}]^{8-}$ (**3a**), have been successfully synthesized by adopting a one-pot reaction strategy. All of these hexatantalates are built from a new-type phosphorus-incorporated hexatantalates. We investigated the solution behaviors, and the peak assignments of the MS spectra indicated some degree of stability of them in water. Furthermore, the proton-conducting ability of compound 1a was also explored and it has shown well conductivity at high relative humidities, with conductivity achieved 1.22×10^{-3} S/cm (85 °C, 90%RH).

Polyoxometalates (POMs) represent an intriguing class of polynuclear metal oxide clusters, which have been attracted widespread attention due to the remarkable properties and varieties of potential applications [1–12]. It is worth noting that POMs have a history of over 100 years and can be divided into two types, iso and hetero-POMs according to whether it contains heteroatoms (typicaly P, As, Sb, Bi) the clusters of V, Mo, W are still relatively mature compared to Nb-based POMs (PONbs) and Ta-based POMs (POTas). Nowdays, PONbs have shown great progress over the past few years thanks to the excellently reported work of Nyman, Cronin, Casey, Wang, Niu and Zheng *et al.* [13–29]. However, the development of POTas, although the first POTa $[Ta_6O_{19}]^{8-}$ has been reported as early as 1953, is still in its budding period [30]. It is attributed to their slower reaction kinetic and higher chemical inertness of Ta. On one hand, the water-soluble precursor $[Ta_6O_{19}]^{8-}$ can only exist steadily among a narrowly strong basicity interval, otherwise $[Ta_6O_{19}]^{8-}$ tend to form gel-like material or Ta_2O_5 precipitate. On the other hand, the alkaline condition impedes the ability to incorporate most metals into the clusters. Up to now, POTas mainly concentrated on the isoPOTas including hexatantalate ions crystallized as simple alkali salts or tetramethylammonium salts [31–34], several organic-inorganic hybrid POTas [35], $\{Ta_7\}$ and $\{Ta_8\}$ cores with organic ligands [36], $\{Ta_{10}\}$ [37], $\{Ti_2Ta_8\}$, $\{Ti_{12}Ta_6\}$ [38] and $\{Co_8Ta_{24}\}$ [39], as well as a series of Ta/W mixed-addendum POTas [40,41]. In 2017, $[P_4Ta_6(O_2)_6O_{25}]^{12-}$ and $[P_4Ta_6\ (O_2)_6O_{24}]^{10-}$ were first proposed by Niu [42], $[Ln1(H_2O_6\ \{H_4(TaO_2)_6As_4O_{24}\})]^{3-}$ (Ln1 = Sm, Eu, Tb, Dy, Er, Tm, Yb, Lu), $[Se_4(TaO_2)_6(OH)_4O_{17}]^{4-}$ and its Ln-derivatives $[Ln(H_2O)_6(TaO_2)_6Se_4(OH)_3O_{18}]^{2-}$ (Ln2 = Tb, Dy, Er, Tm, Yb) were reported in 2019 and 2020 in succession [43]. These complexes were entirely obtained as pure heter-POTa or their lanthanide derivatives. Based on the literature survey, apparently, a large portion of the resulting POTas are in the form of oligomers (mostly dimers). With that, it is still an enormous challenge to make a structural breakthrough for POTas.

Herein, we are reporting three of hetero-POTas, $Cs_3H_3[Ni_2(H_2O)_4\{P_4Ta_6(O_2)_6O_{24}\}]\cdot 7H_2O$ (**1**), $Cs_3NaH_4[Zn(H_2O)_4\{P_4Ta_6(O_2)_6O_{24}\}]\cdot 13H_2O$ (**2**) and $Cs_3NaH_4[Cd(H_2O)_4\ \{P_4Ta_6(O_2)_6O_{24}\}]\cdot 8H_2O$ (**3**) were successfully acquired by adopting a one-post assembly synthetic method. According to Nyman's group, the Lindqvist-type $[Ta_6O_{19}]^{8-}$ can be stabilized as a peroxyanion by H_2O_2 even at a reasonably low pH in aqueous solution [44]. Under this background, we regard the cluster $[P_4Ta_6(O_2)_6O_{24}]^{10-}$ (**P_4Ta_6**) as second building block, and then transition-metal ions were introduced to the reaction system to enrich the structural diversity of POTas. First of all, $K_8Ta_6O_{19}\cdot 17H_2O$ (0.201 g, 0.1 mmol) was dissolved in 20 mL H_2O consisting of 2.0 mL H_2O_2 (30%) with moderate stirring. The pH was adjusted to 1.60 with 3 mol/L H_3PO_4. And then, $NiCl_2\cdot 6H_2O$ (0.156 g, 0.66 mmol) was added slowly. The pH was adjusted to 2.7 with 2 mol/L NaOH and the reaction was heated at 90 °C for 1 h. After that, the mixture was cooled to room temperature and followed by the addition of CsCl (0.01 g, 0.06 mmol). The solution was

* Corresponding authors.
E-mail addresses: jpwang@henu.edu.cn (J. Wang), jyniu@henu.edu.cn (J. Niu).

https://doi.org/10.1016/j.cclet.2021.12.078
1001-8417/

stirred for 30 min and filtered. Finally, the green filtrate was kept in an open beaker to slowly evaporate at room temperature. A similar procedure as **2** and **3** that for the preparation of **1** was used, only changed the type of transition-metal. Crystallographic data and structures refinement for compounds **1**–**3** have been given in Table S1 (Supporting information). As far as we know, this is the first observation about transition-metal containing derivatives in POTa chemisty.

To study the key factors that influence the reaction, a series of parallel experiments have been implemented. The final results indicate that pH value, reaction temperature, the genre of counter cations and transition-mental ions can significantly affect the separation of target products: (1) Crystals of **1**–**3** can be formed in the pH range of 2.1–3.0. At a lower or higher pH, only amorphous products formed with low yield; (2) When the reaction temperature was lower than 70 °C, no crystal was obtained due to the slow kinetics of the reaction; (3) When get rid of Cs^+ or replaced it with other counter cations, only powders were obtained. It is in agreement with the previous conclusion that the nature of the counter cations has a significant impact on the crystallization of POMs [45]; (4) The kind of transition mental element also gives deep impact on the synthesis procedure. In fact, Co^{2+}, $Fe^{2+}$and Cu^{2+}were also tried to lead into the system to obtain isomorphic compounds, but we failed, and only various colors of powder were gained.

Single-crystal X-ray structural analysis reveals that all of the compounds crystallize in the monoclinic system while **1** is in $P2_1/c$ space group, **2** and **3** are in $C2/c$ space group. Compound **1** is isolated, and it comprises a cluster of $[Ni_2(H_2O)_{10}\{P_4Ta_6(O_2)_6O_{24}\}]^{6-}$ (**1a**) (Fig. 1a), three Cs^+ ions and seven water molecules. Compound **1** is captured on equatorial site, the so-called "belt" phosphate group, and another one is capped on axial site, the so-called "cap" phosphate group (Fig. 1d). In **1a**, each Ni atom is ligated by one μ_2-O bridging atom and five water molecules forming an octahedral coordination environment (Fig. S1 in Supporting information). Compounds **2** and **3** are isostructural, thus compound **2** is discussed in detail. **2** comprises a $[Zn(H_2O)_4\{P_4Ta_6(O_2)_6O_{24}\}]^{8-}$ subset (**2a**), three Cs^+ ions, one Na^+ ion and thirteen water molecules. Each Zn atom constructs an octahedral coordination environment by linking with four water molecules and two μ_2-bridging oxygen atoms from two adjacent $\mathbf{P_4Ta_6}$ units (Fig. S1). As shown in Fig. 1b, the sole $\{Zn(H_2O)_4\}$ segment is connected to one belt P atom by μ_2-O bridging atom. Furthermore, every $\{Zn(H_2O)_4\}$ linker bounds together with two moieties $\mathbf{P_4Ta_6}$ by two Zn–O–P bridges, constituting a one-dimensional chain structure, simultaneously, each $\mathbf{P_4Ta_6}$ unit of the 1-D chain is connected to two Na^+ ions, ultimately bringing out an outspread two-dimensional plane framework (Fig. 1c). Compound **3** is fused by the polyanion $[Cd(H_2O)_4P_4Ta_6(O_2)_6O_{24}]^{8-}$ (**3a**) (Fig. S2 in Supporting information), three Cs^+ ions, one Na^+ ion and eight water molecules. Each Ta atom of compounds **1**–**3** is coordinated by three kinds of oxygen atoms: one μ_3-O bridging atom, four μ_2-O bridging atoms and one terminal peroxo group, thus defines a distorted-pentagonal-bipyramidal geometry (Fig. 1e). The Ta–O and Ta–O_p bond length are in the range of 1.91–2.13 Å and 1.92–2.03 Å, respectively. The value of O_p–O_p bond is in the range of 1.48–1.51 Å, mostly greater than 1.50 Å, which is longer comparing to the noncoordinated O_2^{2-} (1.49 Å) [46]. In addition, the transition-metal-oxygen bond lengths are gradually increased, within the range of 1.95–2.12 Å, 2.07–2.13 Å and 2.21–2.34 Å, severally, which agree well with the atoms and ions radius trend of Ni, Zn and Cd centers.

The band valence sum (BVS) [47,48] calculations are carried out on all Ta, P, Ni, Zn, Cd and O centers, and the results indicate that all the Ta, P, Ni, Zn and Cd centers are in +5, +5, +2, +2 and +2 oxidation states, respectively (Table S3 in Supporting information). In addition, the BVS calculations give values of 1.22 and 1.23 for O9, O15 in **1a**, which are relatively lower than those of other oxygen atoms in the structure (1.75–2.18) and further confirm that they appear to be monoprotonated (Table S2 in Supporting information). Meanwhile, the values of terminal oxygen atoms on transition-metal atoms are within the range of 0.63–0.66, indicating that they are from water molecules. The BVS calculation details of **2a** and **3a** are also carried out in Tables S2 and S3 (Supporting information).

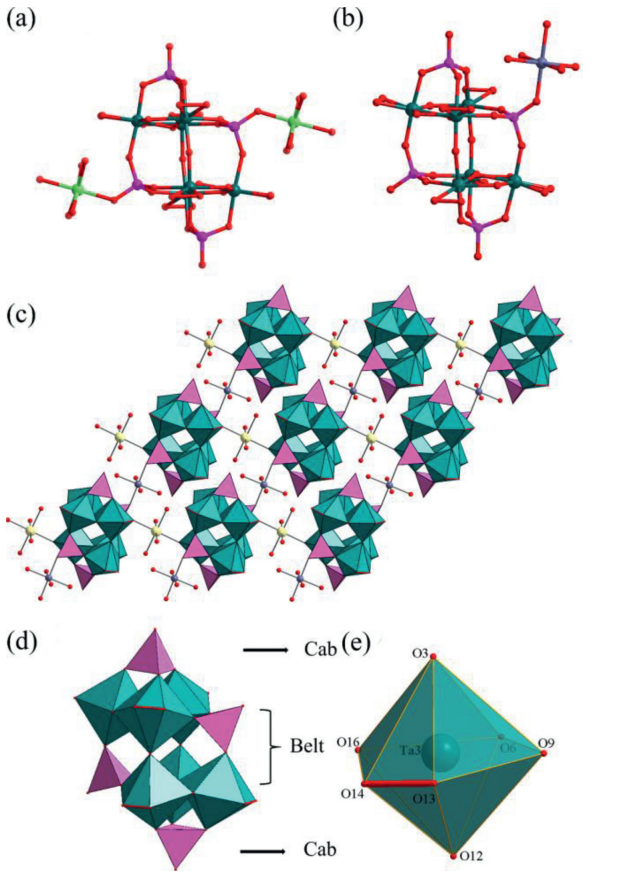

Fig. 1. (a) Ball-and-stick representation of **1a** highlighting the conterminous mode of $\mathbf{P_4Ta_6}$ and Ni atoms. (b) Ball-and-stick representation of **2a**. (c) Polyhedral views of the 2D plane framework of **2**. Color code: TaO_7, turquoise polyhedral; PO_4, rose polyhedral; Ta, dark green spheres; P, rose spheres; Ni, light green spheres; Zn, lilac spheres; Na, light yellow spheres; O, red spheres. (d) Polyhedral representations of $\mathbf{P_4Ta_6}$. (e) The coordination environments of Ta atom.

We have already known that the crystal sample of the anion $[P_4Ta_6(O_2)_6O_{24}]^{10-}$ is colorless (white after weathering), and when the Ni, Zn and Cd atoms were incorporated into the anion $[P_4Ta_6(O_2)_6O_{24}]^{10-}$, the color of compounds **1**–**3** were green, colorless and colorless (Fig. S13 in Supporting information). It might be owing to the different valence electrons—$3d^84s^2$, $3d^{10}4s^2$ and $4d^{10}5s^2$ for Ni, Zn and Cd atoms. Meanwhile, we also compared compounds **1**–**3** with $[P_4Ta_6]$ cluster in solid-UV–vis absorption (Fig. 2). The results indicated compounds **1**–**3** and $[P_4Ta_6]$ cluster have similar absorption peaks in around 250 nm, which can be attributed to the charge-transfer transitions of oxygen-to-tantalum bonds. Besides, the absorption peaks in around 408 nm and 700 nm of compound **3** can be assigned to be d–d transfers of incorporated 3d Ni^{2+} ion [49].

To investigate the solution behavior of compounds **1**–**3**, negative-mode electrospray ionization mass spectrometry (ESI-MS) analysis were examined in aqueous solution (Fig. S14 in Supporting information). For compound **1**, the ESI-MS shows two envelopes that correspond to the intact cluster at charge value

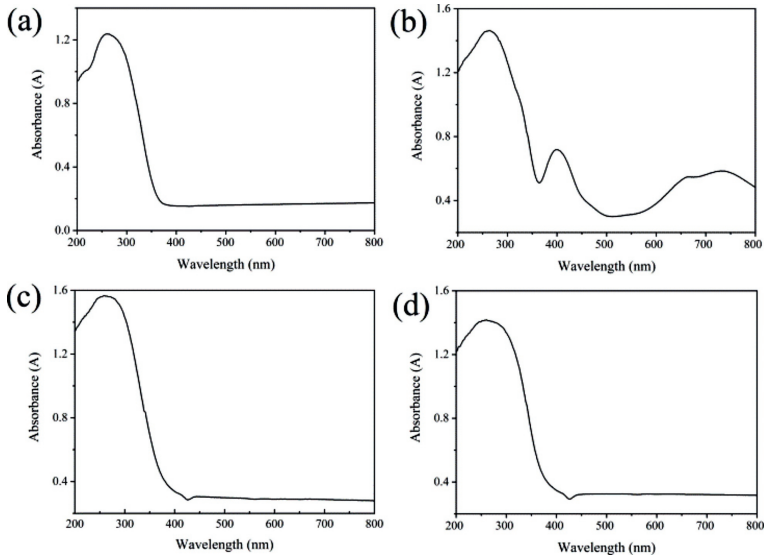

Fig. 2. The solid-UV–vis curve of (a) [P_4Ta_6] cluster, (b) **1**, (c) **2** and (d) **3**.

Table 1
Assignment of the key species identified of ESI-MS tests for **1**.

Peaks assignment	Charges	Calcd. *m/z*	Exp. *m/z*
$\{H_7P_4Ta_6(O_2)_6O_{24}\}$	−3	597.47	597.51
$\{H_7P_4Ta_6(O_2)_6O_{24}(H_2O)\}$	−3	604.17	604.11
$\{H_5[NiP_4Ta_6(O_2)_6O_{24}]\}$	−3	616.11	616.12
$\{H_3[Ni_2(H_2O)_4P_4Ta_6(O_2)_6O_{24}]\}$	−3	660.11	660.09
$\{H_8P_4Ta_6(O_2)_6O_{24}\}$	−2	896.72	896.73
$\{H_6[Ni_2(H_2O)P_4Ta_6(O_2)_6O_{24}]\}$	−2	962.67	962.71

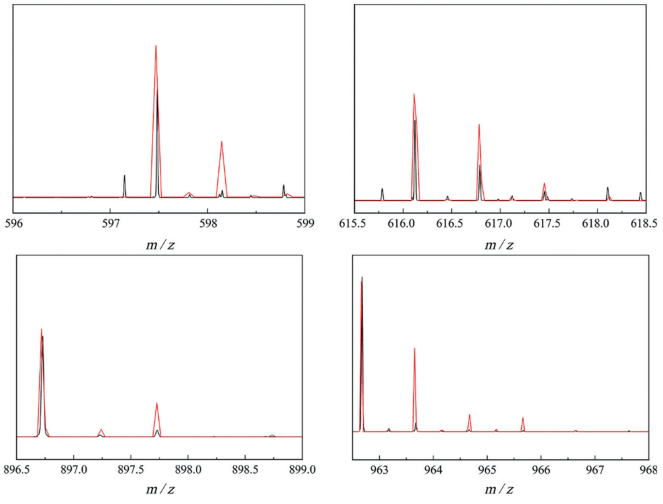

Fig. 3. Simulated (red) and experimental (black) negative-mode mass spectra of isotopic envelopes for **1**.

of 3– and 2– at *m/z* 616.11 $\{H_5[NiP_4Ta_6(O_2)_6O_{24}]\}$ and 962.67 $\{H_6[Ni_2(H_2O)P_4Ta_6(O_2)_6O_{24}]\}$ (Table 1), and that simulated and experimental negative-mode mass spectra of isotopic envelopes for **1** in Fig. 3; for compound **2**, the peaks at the charge values of 3– and 2– of *m/z* 618.79 $\{H_5[ZnP_4Ta_6(O_2)_6O_{24}]\}$ and 927.69 $\{H_6[ZnP_4Ta_6\ (O_2)_6O_{24}]\}$ (Table S4) can be attributed to the stable cluster; for compound **3**, the peaks at the value of *m/z* 634.43 $\{H_5[CdP_4Ta_6(O_2)_6O_{24}]\}$ and 951.62 $\{H_6[CdP_4Ta_6(O_2)_6O_{24}]\}$, at a charge of 3– and 2–, ascribing to the complete configuration (Table S5 in Supporting information). Some other signals around

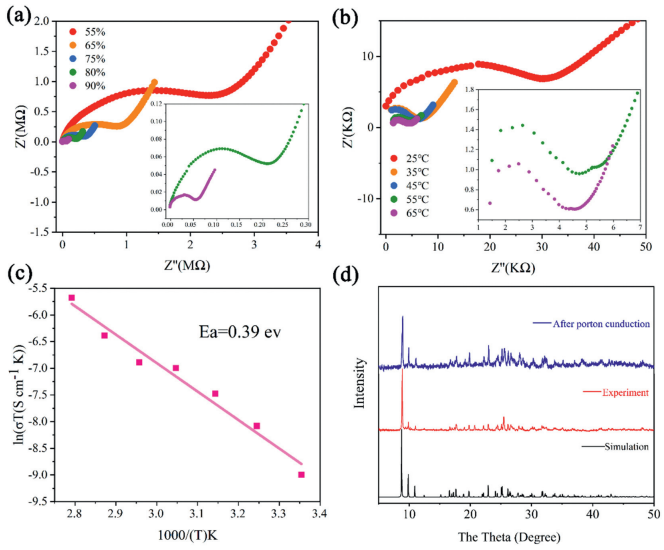

Fig. 4. (a) Nyquist plots **1** under different RHs at 25 °C. (b) Nyquist plots **1** at 90% RH under different temperatures. (c) Arrhenius plot at 75% RH within the temperature range of 25 °C to 85 °C. (d) PXRD patterns of **1**: experiment, simulated and post proton conduction.

can also be found, and they are contributed to the fragment $\mathbf{P_4Ta_6}$ species. Theoretical calculations could provide additional confirmation (Figs. S17 and S18 in Supporting information). The peak assignments of the MS spectra indicate some degree of stability of **1**–**3** in water.

The presence of protonated H^+ and the incorporation of water molecules within the framework prompted us to study the proton-conducting ability. Here the proton conductivity of compound **1** was investigated. First, the proton conductivity was tested on the humidity (RH) from 55% to 90% at room temperature. As shown in Fig. 4a, the conductivity σ (which was calculated by the equation $\sigma = L/RS$, where L is the sample thickness, S is the cross-sectional area, and R represents the resistance) was increased from 7.26×10^{-7} S/cm to 3.69×10^{-5} S/cm [50,51]. Then, the temperature-dependent conductivity was carried out in the

range of 25 °C to 85 °C, and the conductivity ranging from 3.69×10^{-5} S/cm to 1.22×10^{-3} S/cm (Fig. 4b). These phenomena instruct that the increase of conductivity was coordinated by RH and temperature.

According to the Arrhenius equation ($\sigma T = \sigma_0 \exp(E_a/k_b T)$, the activation energies (E_a) are derived to be 0.39 eV. In general, the mechanism of proton conductivity should be assigned to the Grotthuss mechanism ($E_a = 0.1$–0.4 eV) (Fig. 4c). In order to confirm the integrity of the structure of **1** proton conduction experiments, powder X-ray diffraction experiment was carried out (Fig. 4d). It turns out that the PXRD curve post the proton conductivity tests aligns with that from the original form. The thermal stability of compound **1** was characterized by PXRD at different temperatures (Fig. S19 in Supporting information).

In summary, three new compounds have been successfully obtained and fully investigated in the solid state by single-crystal X-ray diffraction, IR spectra, TGA, PXRD and the solution behavior as well as proton conductivity. To date, it is the first study about transition-metal incorporated peroxo-polyoxotantalate, which not only enriches the diversity of POTas but also provides further insight into the reactivity between alkalineside POTas and transition metals under strong acidic conditions in the presence of H_2O_2. Moreover, the appropriate reaction conditions make important sense to the formation of aggregations. In addition, the excellent proton conductivity shows that POTas has enormous potential in the application of materials.

Declaration of competing interest

The authors declare that they have no known competing financial interests or personal relationships that could have appeared to influence the work reported in this paper.

Acknowledgments

This work was funded by the National Natural Science Foundation of China (Nos. 22171071, 22071044, 21771054 and 21571050).

Supplementary materials

Supplementary material associated with this article can be found, in the online version, at doi:10.1016/j.cclet.2021.12.078.

References

[1] A. Merca, S. Garai, A. Müller, et al., Angew. Chem. Int. Ed. 52 (2013) 11765–11769.
[2] Y.N. Gu, Y. Chen, X.X. Li, et al., Inorg. Chem. 57 (2018) 2472–2479.
[3] Y. Zhu, P. Yin, F. Xiao, et al., J. Am. Chem. Soc. 135 (2013) 17155–17160.
[4] J. Gao, J. Miao, Q. Zhang, et al., Dalton Trans. 44 (2015) 14354–14358.
[5] G.P. Yang, X.L. Zhang, Y.F. Liu, et al., Inorg. Chem. Front. 8 (2021) 4650–4656.
[6] L. Qiao, M. Song, A. Geng, S. Yao, Chin. Chem. Lett. 30 (2019) 1273–1276.
[7] S.T. Zheng, G.Y. Yang, Chem. Soc. Rev. 41 (2012) 7623.
[8] Z. Sun, H.Z. Bie, Y. Wu, et al., Chin. Chem. Lett. 24 (2013) 76–78.
[9] G.P. Yang, K. Li, X.L. Lin, et al., Chin. J. Chem. 39 (2021) 3017–3022.
[10] A. Dolbecq, E. Dumas, C.R. Mayer, P. Mialane, Chem. Rev. 110 (2010) 6009–6048.
[11] M. Cheng, Y. Liu, D. Zhang, et al., Chin. Chem. Lett. (2021), doi:10.1016/j.cclet.2021.11.059.
[12] M. Lv, Y. Liu, K. Li, G. Yang, Tetrahedron Lett. 65 (2021) 152757.
[13] Z. Liang, L. Zhang, J. Wang, Inorg. Chem. 58 (2019) 27–30.
[14] L. Li, K. Dong, J. Wang, et al., Chem. Eur. J. 23 (2017) 16957–16960.
[15] Z. Liang, D. Zhang, J. Niu, et al., Chem. Eur. J. 21 (2015) 8380–8383.
[16] S. Chen, P. Ma, J. Wang, Chem. Commun. 53 (2017) 3709–3712.
[17] J. Niu, P. Ma, J. Wang, et al., Chem. Eur. J. 13 (2007) 8739–8748.
[18] Y. Wu, X. Li, S. Zheng, Angew. Chem. Int. Ed. 57 (2018) 8572–8576.
[19] L. Jin, Z.K. Zhu, S.T. Zheng, Angew. Chem. Int. Ed. 56 (2017) 16288–16292.
[20] J.H. Son, D.H. Park, D.A. Keszler, W.H. Casey, Chem. Eur. J. 21 (2015) 6727–6731.
[21] Z.Y. Zhang, J. Peng, et al., Chem. Commun. 51 (2015) 3091–3093.
[22] H.L. Wu, Z.M. Zhang, Y.G. Li, X.L. Wang, E.B. Wang, CrystEngComm 17 (2015) 6261–6268.
[23] J.H. Son, W.H. Casey, Chem. Commun. 51 (2015) 1436–1438.
[24] Y. Hou, L.N. Zakharov, M. Nyman, J. Am. Chem. Soc. 135 (2013) 16651–16657.
[25] J.Q. Shen, S. Yao, Z.M. Zhang, et al., Dalton Trans. 42 (2013) 5812.
[26] Y. Hou, T.M. Alam, M.A. Rodriguez, M. Nyman, Chem. Commun. 48 (2012) 6004.
[27] R.P. Bontchev, M. Nyman, Angew. Chem. 118 (2006) 6822–6824.
[28] M. Nyman, A.J. Celestian, J.B. Parise, G.P. Holland, T.M. Alam, Inorg. Chem. 45 (2006) 1043–1052.
[29] M. Nyman, F. Bonhomme, T.M. Alam, J.B. Parise, G.M.B. Vaughan, Angew. Chem. Int. Ed. 43 (2004) 2787–2792.
[30] I. Lindqvist, B. Aronsson, Ark. Kemi 7 (1954) 49–52.
[31] M. Matsumoto, Y. Ozawa, A. Yagasaki, Inorg. Chem. 51 (2012) 5991–5993.
[32] M. Matsumoto, Y. Ozawa, A. Yagasaki, Inorg. Chem. Commun. 14 (2011) 115–117.
[33] L. Shen, Y.Q. Xu, Y.Z. Gao, F.Y. Cui, C.W. Hu, J. Mol. Struct. 934 (2009) 37–43.
[34] M. Nyman, T.M. Anderson, P.P. Provencio, Cryst. Growth. Des. 9 (2009) 1036–1040.
[35] P.A. Abramov, M.N. Sokolov, V.P. Fedin, et al., Dalton Trans. (44) (2015) 2234–2239.
[36] I. Abrahams, D.C. Bradley, H. Chudzynska, M. Motevalli, P. O'Shaughnessy, J. Chem. Soc. Dalton Trans. (2000) 2685–2691.
[37] M. Matsumoto, Y. Ozawa, A. Yagasaki, Y. Zhe, Inorg. Chem. 52 (2013) 7825–7827.
[38] J.H. Son, W.H. Casey, Chem. Eur. J. 22 (2016) 14155–14157.
[39] Z. Liang, S. Zhao, P. Ma, C. Zhang, et al., Inorg. Chem. 57 (2018) 12471–12474.
[40] S.J. Li, S.M. Liu, J.H. Ye, et al., J. Am. Chem. Soc. 134 (2012) 19716.
[41] P. Huang, C. Qin, Z.M. Su, et al., Chem. Commun. 52 (2016) 13787.
[42] D. Zhang, Z. Liang, J. Niu, et al., Inorg. Chem. 56 (2017) 5537–5543.
[43] Z. Liang, H. Wu, J. Wang, et al., Inorg. Chem. 58 (2019) 13030–13036.
[44] L.B. Fullmer, C.E. Malmberg, M. Nyman, et al., Dalton Trans. 46 (46) (2017) 8486–8493.
[45] C.P. Pradeep, D.L. Long, L. Cronin, Dalton Trans. 39 (2010) 9443.
[46] S.C. Abrahams, R.L. Collin, W.N. Lipscomb, Acta Cryst. 4 (1951) 15–20.
[47] D. Brown, D. Altermatt, Acta Cryst, Sect. B 41 (1985) 244.
[48] H.H. Thorp, Inorg. Chem. 31 (1992) 1585.
[49] F.A. Cotton, G. Wilkinson, C.A. Murillo, M. Bochmann, Advanced Inorganic chemistry, 6th.ed., Wiley, New York, 1999.
[50] D.W. Lim, H. Kitagawa, Chem. Rev. 120 (2020) 8416–8467.
[51] W.H. Wang, Q. Gao, X.H. Bu, et al., Chin. Chem. Lett. 29 (2018) 336–338.